

Cylindrical phase of diblock copolymers confined in thin films. A real-space self-consistent field theory study

Yingzi Yang, Feng Qiu*, Hongdong Zhang, Yuliang Yang

The Key Laboratory of Molecular Engineering of Polymers, Ministry of Education, Department of Macromolecular Science, Fudan University, Shanghai 200433, China

Received 7 November 2005; received in revised form 27 December 2005; accepted 16 January 2006
Available online 7 February 2006

Abstract

We have used real-space self-consistent field theory to search possible morphology of an asymmetric AB diblock copolymer thin film confined between two homogeneous hard walls. The volume fraction of the A block is fixed to be $f=0.3$, as expected, a cylindrical phase is stable without confinement (in the bulk). Our simulation reveals that under confinement, in addition to parallel and perpendicular cylinders, other phases, such as flat lamellae, perforated lamellae, undulated cylinders and undulated lamellae, are also stable due to the block–substrate interactions. Three new structures, i.e. undulated lamellae, undulated cylinders and parallel cylinders with non-integer period, are observed to be stable with suitable film thickness and block–substrate interaction. By systematically varying the film thickness and the interaction parameters between the two blocks, phase diagrams are constructed for typical block–substrate interactions. We compare the phase diagrams for weak and strong substrate preference and discuss the effects of confinement and substrate preference on the stability of various structures.

© 2006 Elsevier Ltd. All rights reserved.

Keywords: Diblock copolymer; Self-consistent mean-field theory; Thin films

1. Introduction

Two or more distinct polymer chains jointed chemically at their ends form block copolymers, which prevent macrophase separation of different species and can self-assemble into complex nano-scale morphologies. After four decades of intensive experimental and theoretical investigations, it has been recognized that for AB diblock copolymers in the bulk only four microphases—lamella, gyroid, cylinder, and sphere—are thermodynamically stable. When confined in thin films, diblock copolymers demonstrate much more complicated structures, which have attracted much recent experimental and theoretical attention.

The confined thin films of symmetric diblock copolymers (with the equal volume fraction of the two species) have been extensively studied in experiments [1–7], simulations [8–14], and theories [8,15–23]. Their phase behavior has been understood fairly well. When the substrates are neutral to both species, the lamellae phase that are perpendicular to

the substrates are always stable; however, when the substrates have a slight preference of one species, the microphases alternate between parallel and perpendicular lamellae as the thickness of the thin film increases. With this accomplishment in hand, researchers recently turned to films of asymmetric diblock copolymers. The experimental [24–36] and theoretical [8,37–43] studies which focused on thin films of $f\approx 0.3$ diblock copolymers (where f is the volume fraction of the A species) emerged. Under confinement, diblock copolymers with cylindrical phase in the bulk may not only change the orientation of the cylinders, but also alternate between different morphologies, provided suitable polymer–substrate interaction energy and film thickness. Recently, the phase behavior of cylinder-forming triblock copolymer under thin films conditions attracts much attention [44–49].

The experiments on asymmetric diblock copolymer thin films began a decade ago. And Monte–Carlo simulation and dynamic density functional theory (DDFT) [38–40] on equilibrium states in thin films have been carried out, with a good agreement with experiments. The focus of recent computer simulations is: (a) substrate property [42,47,49], i.e. the systems with upper and lower substrates having different preference to the blocks or there being some decorated pattern on the substrates; (b) surface reconstruction [44,46,47,49], i.e. wetting layer and the nearest two molecular

* Corresponding author.

E-mail address: fengqiu@fudan.edu.cn (F. Qiu).

layers against substrates being carefully examined; (c) hybrid structures [46–48], i.e. under confinements, different structures occurring in different horizontal layers, in the same horizontal layer, or connected with each other.

To get a complete picture of the phase behavior of asymmetric diblock copolymer confined in thin films, in this paper, we perform extensive simulations using the real-space self-consistent field theory (SCFT) for polymers, which has the advantage on reaching complicated structures in equilibrium states. We focus on a typical asymmetric diblock composition $f=0.3$ and assume the two confining substrates are homogenous, hard, and selective, which attract one component while repel another. As expected, previously reported structures, such as parallel lamellae, perforated lamellae, perpendicular and parallel cylinders, are observed. Moreover, new structures, such as undulated lamellae, undulated cylinders and cylinders with non-integer period, are unearthed in the present work, and are proved to be stable under particular conditions.

The paper is organized as follows. In Section 2, we briefly describe the model and the theory we used. In Section 3 we first present the morphology uncovered and then discuss the phase diagram of the confined diblock copolymer with various block–substrate interactions. Section 4 is devoted to conclusions.

2. Model and theory

We consider a system of n AB diblock copolymer melt with volume V . Each polymer has the same chain length N and the composition f . We assume that the A and B segments have equal statistical segment length a . The melt system is confined between two hard, flat walls and the distance between them is Δ .

The SCFT for confined block copolymers has been developed previously [20]. We briefly describe it as follows. To cope with a many-body system, (mean) fields conjugated to local segment densities are introduced,

$$w_A(\vec{r}) = \chi_{AB}N\Phi_B(\vec{r}) - H(\vec{r})N + \xi(\vec{r}) \quad (1)$$

$$w_B(\vec{r}) = \chi_{AB}N\Phi_A(\vec{r}) + H(\vec{r})N + \xi(\vec{r}) \quad (2)$$

where $H(\vec{r})N$ is a surface field,

$$H(\vec{r}) = \begin{cases} \frac{1}{4}A_1(1 + \cos(\pi z/\varepsilon)) & 0 \leq z \leq \varepsilon \\ 0 & \varepsilon \leq z \leq \Delta - \varepsilon \\ \frac{1}{4}A_2(1 + \cos(\pi(\Delta - z)/\varepsilon)) & \Delta - \varepsilon \leq z \leq \Delta \end{cases} \quad (3)$$

z is the coordinate perpendicular to the film. ε denotes the thickness of the surfaces. $A_1 = -(\chi_{AS_1} - \chi_{BS_1})$ and $A_2 = -(\chi_{AS_2} - \chi_{BS_2})$ (with χ_{AS_1} , χ_{BS_1} , χ_{AS_2} , and χ_{BS_2} , denoting the interactions between the blocks and substrates) control the strength of the interaction between the polymer and the substrates at the $z=0$ and Δ surfaces. We assume positive A_1

and A_2 values favor the segregation of the A blocks to the substrates.

In Eqs. (1) and (2), $\Phi_A(\vec{r})$ and $\Phi_B(\vec{r})$ are local densities of the species A and B. $\xi(\vec{r})$ is the field to ensure the incompressibility, which is determined by,

$$\Phi_A(\vec{r}) + \Phi_B(\vec{r}) = \Phi(\vec{r}) \quad (4)$$

In the bulk, $\Phi(\vec{r})$ always equals to 1, independent of position \vec{r} . Near the confined boundaries, from the melt to the hard walls, $\Phi(\vec{r})$ decays from 1 to 0. To simplify the calculation, we define it to be 1/2 in the surface layers,

$$\Phi(z) = \begin{cases} \frac{1}{2}, & 0 \leq z \leq \varepsilon \\ 1, & \varepsilon < z < \Delta - \varepsilon \\ \frac{1}{2}, & \Delta - \varepsilon \leq z \leq \Delta \end{cases} \quad (5)$$

Thus, the value of $H(\vec{r})$ is,

$$H(\vec{r}) = \begin{cases} \frac{1}{4}A_1 & 0 \leq z \leq \varepsilon \\ 0 & \varepsilon \leq z \leq \Delta - \varepsilon \\ \frac{1}{4}A_2 & \Delta - \varepsilon \leq z \leq \Delta \end{cases} \quad (6)$$

In SCFT the free energy of the system F can be written as,

$$\begin{aligned} \frac{F}{nk_B T} = & -\ln\left(\frac{Q}{V}\right) + \frac{1}{V} \int d^3\vec{r} \chi_{AB}N\Phi_A(\vec{r})\Phi_B(\vec{r}) \\ & - \frac{1}{V} \int d^3\vec{r} \{w_A(\vec{r})\Phi_A(\vec{r}) + w_B(\vec{r})\Phi_B(\vec{r})\} \\ & - \frac{1}{V} \int d^3\vec{r} \xi(\vec{r})\{\Phi_0(\vec{r}) - \Phi_A(\vec{r}) - \Phi_B(\vec{r})\} \\ & - \frac{1}{V} \int d^3\vec{r} H(\vec{r})N\{\Phi_A(\vec{r}) - \Phi_B(\vec{r})\} \end{aligned} \quad (7)$$

where Q is the partition function of a single chain,

$$Q = \int q(s, \vec{r})q^+(s, \vec{r})d\vec{r} \quad (8)$$

where $q(s, \vec{r})$ and $q^+(s, \vec{r})$ can be solved by two modified diffusion equations,

$$\frac{\partial}{\partial s} q(s, \vec{r}) = \frac{a^2 N}{6} \nabla^2 q(s, \vec{r}) - w(s, \vec{r})q(s, \vec{r}) \quad (9)$$

$$\frac{\partial}{\partial s} q^+(s, \vec{r}) = -\frac{a^2 N}{6} \nabla^2 q^+(s, \vec{r}) + w(s, \vec{r})q^+(s, \vec{r}) \quad (10)$$

where s is a parameter increasing continuously from 0 to 1 along the chain, starting from the A head and ending at the B end. The initial conditions of the above equations are $q(s=0, \vec{r}) = 1$ and $q^+(s=1, \vec{r}) = 1$. The mean field is

defined as,

$$w(\vec{r}, s) = \begin{cases} w_A(\vec{r}, s), & 0 \leq s \leq f \\ w_B(\vec{r}, s), & f \leq s \leq 1 \end{cases} \quad (11)$$

The local segment density can be calculated by

$$\Phi_A(\vec{r}) = \frac{V}{Q} \int_0^f q(s, \vec{r}) q^+(s, \vec{r}) ds \quad (12)$$

$$\Phi_B(\vec{r}) = \frac{V}{Q} \int_f^1 q(s, \vec{r}) q^+(s, \vec{r}) ds \quad (13)$$

Eqs. (1), (2), (4), (12) and (13) form a closed set of self-consistent equations. To solve these equations, at first initiate random fields $w_A(\vec{r})$ and $w_B(\vec{r})$ are given, we then evaluate the two partition functions $q(s, \vec{r})$ and $q^+(s, \vec{r})$ by solving Eqs. (9) and (10) with the alternative direction implicit method. The density fields are evaluated by Eqs. (12) and (13). With the obtained segment density, the fields are updated by a combination of their old and new values according to Eqs. (1) and (2). With the new fields, the partition functions $q(s, \vec{r})$ and $q^+(s, \vec{r})$ are evaluated again to obtain the segment density. These steps are iterated until the required self-consistency is reached [50] and the free energy is minimized. To avoid the influence of the simulation box size in the x - and y -directions, each minimization of the free energy is iterated with respect to a variety of reasonable sizes in the x - and y -directions. In order to avoid the real space method becoming trapped in a metastable state, random noises are added on the fields to disturb the morphology formed in the iterations. Furthermore, each minimization is run several times using different initial random guesses of the potential fields $w_A(\vec{r})$ and $w_B(\vec{r})$ to ensure that the exact equilibrium morphology has been obtained. In this fashion, both typical ordered morphologies and the phase diagram for confined block copolymers can be obtained by systematically changing the values of the parameters.

3. Results and discussion

The confined AB diblock copolymer film system is specified by six parameters: f , Δ , N , χ_{AB} , A_1 , and A_2 . In our simulation, we fix $N=50$, $f=0.3$ and vary $\chi_{AB}N=20-40$, which corresponds to cylindrical phase in bulk [51]. The chain length used is long enough for a reasonable description of the complicated microphase structures. The calculation is carried out on a three-dimensional $L_x \times L_y \times L_z$ lattice, with periodic boundary condition in the x - and y -directions. The z -direction is normal to the film surfaces and $L_z = \Delta$ denotes the thickness of the film. In the lattice box, we set the statistical segment length a to be $\sqrt{2}/2$, thus the statistical end-to-end distance of the Gaussian chain is $R_{\text{Gauss}} = aN^{1/2} = 5$. We choose $\epsilon/aN^{1/2} = 0.20$. Again, to simplify the calculation, we assume that the property of the two substrates are symmetric, so that $A = A_1 = A_2$. $A > 0$

means an attractive effect for the segment A toward the substrates and a repellent effect for the segment B; while $A < 0$ means an repellent effect for A and an attractive effect for B. Undoubtedly, with the symmetric substrates condition, certain mixed phase structures will be lost, but in this paper we only focused on thin films between two hard walls of the same property. Finally, our parameters are reduced to three: Δ , $\chi_{AB}N$ and A .

The enrichment of one component near substrates usually corresponds to a separate wetting layer [44–47,49]. But in our simulation, considering the range of the film thickness and the structure of wetting layers, we identify different microphases found in the simulation by visual assessment of the density profile including wetting layers, to facilitate comparing structures under different surface property. Compared with symmetric diblock copolymer thin films, the asymmetric ones show much more complicated structures. We classify these morphologies into four primary classes: cylinders (C), lamellae (L), perforated lamellae (P), and hybrid structures (H), with each class containing several kinds of related structures.

- (1) *Cylinders*. Although cylinders are the bulk phase when $f=0.3$, they are not always dominant in thin films. Three kinds of cylinders are found in our screening, shown in Fig. 1:
 - A. *Perpendicular cylinders* (C_{\perp}). The cylinders are perpendicular to the substrates and arranged in a hexagonal lattice.
 - B. *Parallel cylinders* (C_{\parallel}). The cylinders are parallel to the substrates. We have $1C_{\parallel}$, $1.5C_{\parallel}$ and $2C_{\parallel}$. The numbers on the left denotes the number of layers of cylinders in the thin film counted in the z -direction. Note half layer (non-integer period) is possible.
 - C. *Undulated cylinders* (C_u). The cylinders are not straight, but undulated between two surfaces, and the peaks of neighboring cylinders are interlaced.
- (2) *Lamellae*. If the surface interaction energy between the polymers and substrates dominates, lamellae structure could be more favorable than cylinders. There are two kinds of lamellae found, shown in Fig. 2:
 - A. *Flat lamellae* ($1L_f$, $2L_f$). The interfaces of the A and B components are flat planes parallel to the substrates. The numbers on the left denotes the number of period in the thin film counted in the z -direction.
 - B. *Undulated lamellae* ($1L_u$, $2L_u$). The interfaces of the A and B components are undulated. The waves are arranged in particular patterns, such as linear or square lattices (Fig. 2, $1L_u$ (a), (b), the color pattern on the surface denotes the local density of the segment A. The density decreases from red to green area). The free energies of these different patterns are very close to each other.
- (3) *Perforated lamellae*. Perforated lamellae structure (P) is proven to be metastable in the bulk phase by strong segregation theory and SCFT. But it is stable under thin film conditions, due to the confinement and preference of the substrates, as shown in Fig. 3.

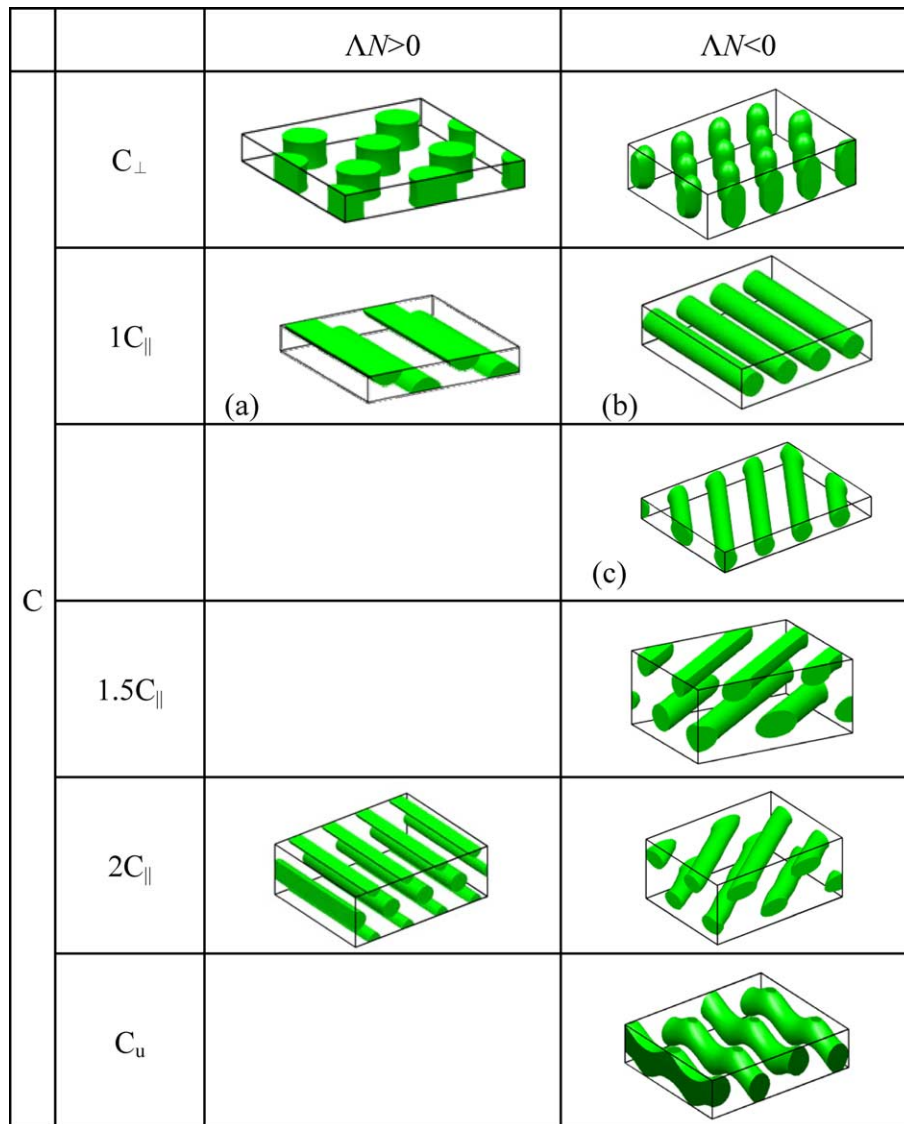


Fig. 1. Cylindrical structures under confinement.

(4) *Hybrid structures.* We have also found stable, hybrid structures of cylinders, lamellae, and perforated lamellae. We use two letters together to denote the types of the mixture. For example, LC means a mixed structure of lamellae and cylinders. In Fig. 4, only a few kinds of these complicated phases are shown.

These structures, such as the perpendicular cylinders, parallel cylinders with integer number of layers, flat lamellae, and perforated lamellae, have also been observed in previous experiments and simulations [24–33,44–49]. However, the undulated lamellae and cylinders, as well as parallel cylinders with fractional number (non-integer) of layers are found for the first time in the present real-space SCFT calculation. Although in Ref. [47], Lyakhova et al. had mentioned the shape modulation in cylinders, the cylinders they found form undulation at one side of the film with the changing sectional area since they assumed the asymmetric substrates; while we have undulated cylinders which have uniform section and form

undulation at each side of the film with symmetric substrates, as shown in Fig. 1.

These new structures we mentioned above are proved to be stable by comparing their free energy with other different structures. We present four typical $\chi_{AB}N-\Delta$ phase diagrams (Figs. 5–8), classified into two classes: the weak and strong substrate preferences. The phase diagram is more complicated than one has expected.

The transformation between the morphologies is the result of the competition between two factors—the entropy and the short-range interaction. In Eq. (7), the first term on right-hand side is the entropic free energy, and the followings are the short-range interaction between segments themselves as well as segments and substrates. Since entropy is a key factor to characterize the radius of gyration of chains, we plot Fig. 9 to show the entropic energy under thin-film confinement when $\chi N=25$, $\Delta N=-8.0$ and $f=0.3$. The horizontal coordinate is the film thickness Δ , while the vertical coordinate is the entropic free energy $-\ln(Q/Q_0)$,

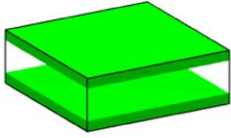
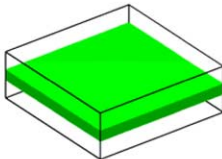
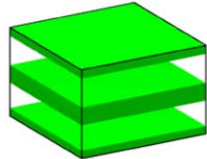
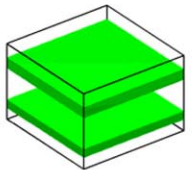
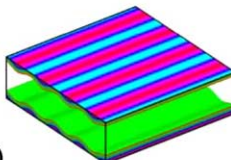
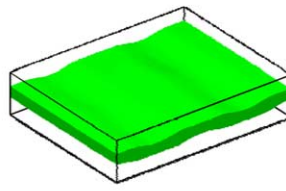
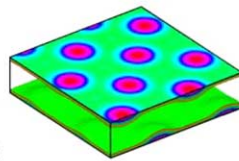
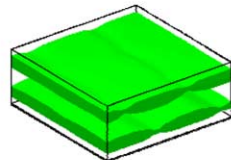
		$\Delta N > 0$	$\Delta N < 0$
L	$1L_f$		
	$2L_f$		
	$1L_u$	(a) 	
		(b) 	
	$2L_u$		

Fig. 2. Lamellar structures under confinement. The surface color in $1L_u$ (a) and (b) shows the concentration fluctuations.

comparing with the bulk entropic free energy. Q_0 is the entropy of a single chain in bulk. The curve is above the zero line and it decays with the thickness. That means under the thin-film condition, the chains are always compressed

compared to the phase-separated bulk case. The compression can be released if the film thickness increases. We can expect the curve to approach zero when the film is thick enough and the compression is small enough to be neglected.

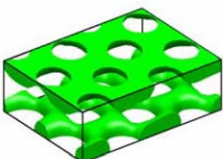
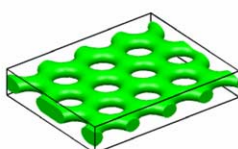
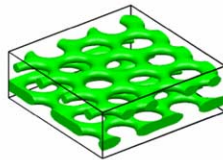
		$\Delta N > 0$	$\Delta N < 0$
P	$1P$		
	$2P$		

Fig. 3. Perforated lamellae under confinement.

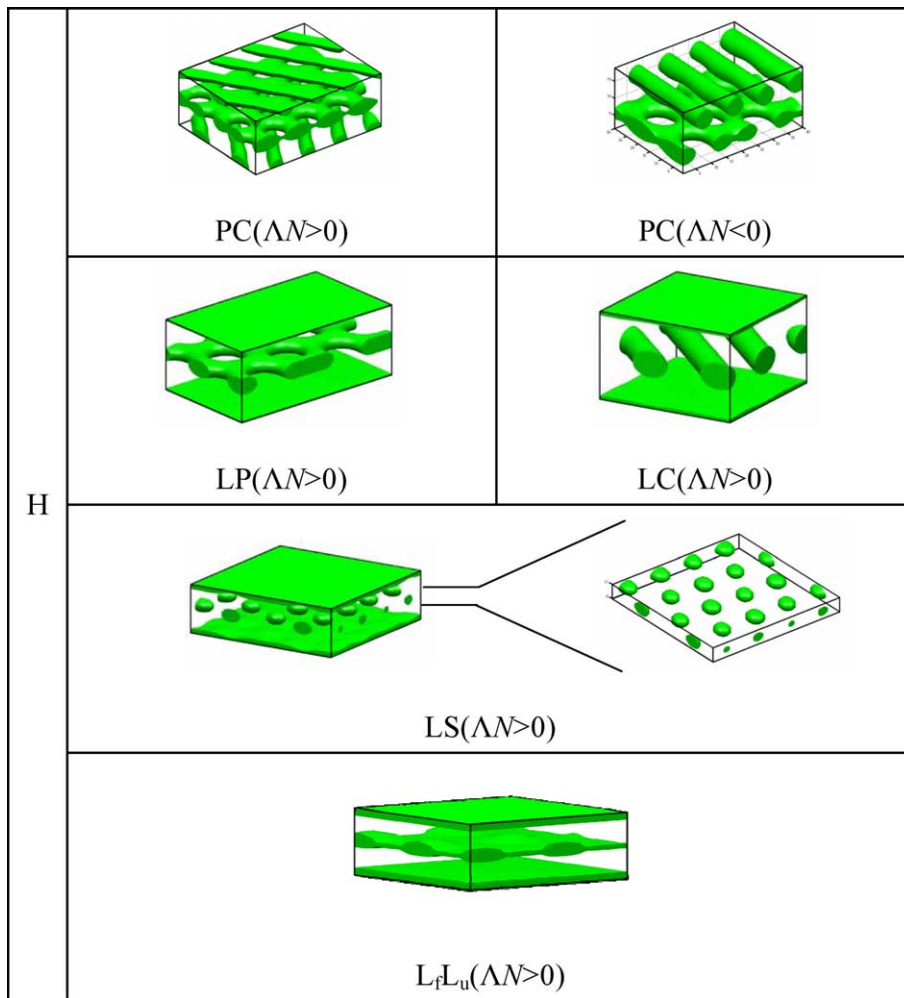


Fig. 4. Hybrid structures under confinement.

Furthermore, the entropic energy depends on the morphology. In Fig. 9, the curve has a minimum at $\Delta = 3.0R_{Gauss}$, corresponding to C_{\perp} , which is the morphology of the most adjacent periodicity to the bulk.

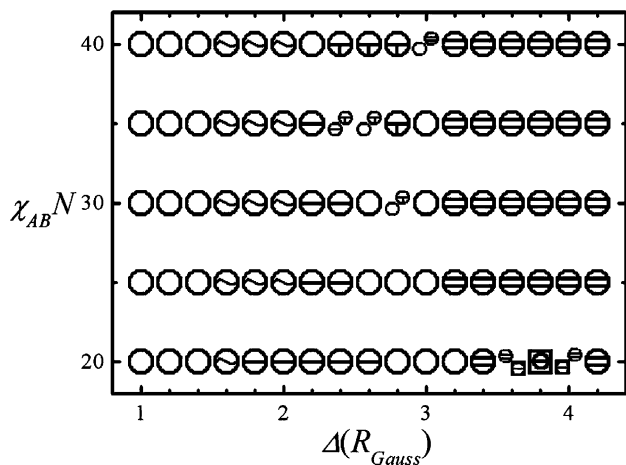


Fig. 5. Phase diagram for $\Delta N = -8.0$. $\odot C_{\perp}$, $\ominus C_u$, $\ominus 1C_{\parallel}$, $\oplus 1.5C_{\parallel}$, $\ominus 2C_{\parallel}$, $\boxtimes PC$, $\oplus 1C_{\parallel}$ and $1.5C_{\parallel}$ with same free energy, $\oplus C_{\perp}$ and $1.5C_{\parallel}$ with same free energy, $\oplus C_{\perp}$ and $2C_{\parallel}$ with same free energy, $\oplus PC$ and $2C_{\parallel}$ with the same free energy.

3.1. Weak substrate preference

In the following, we use a combined parameter ΔN to denote the substrate–block interaction. We choose $\Delta N = \pm 8.0$ for the weak substrate preference case, since Δ is the difference

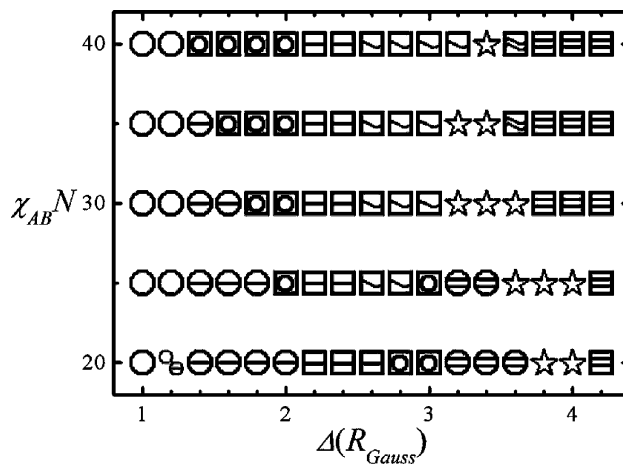


Fig. 6. Phase diagram for $\Delta N = 8.0$. $\odot C_{\perp}$, $\ominus 1C_{\parallel}$, $\boxtimes 1P$, $\boxtimes 1L_r$, $\boxtimes 1L_u$, $\ominus 2C_{\parallel}$, $\boxtimes 2L_r$, $\boxtimes 2L_u$, $\star H$.

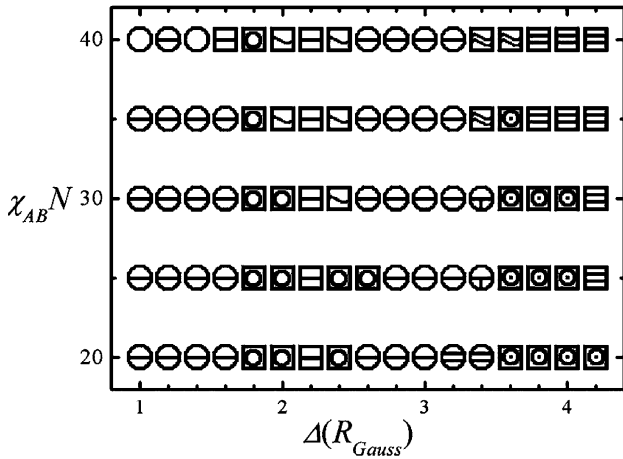


Fig. 7. Phase diagram for $\Delta N = -40.0$. $\circ C_{\perp}$, $\ominus 1C_{\parallel}$, $\boxplus 1L_f$, $\boxminus 1P$, $\boxplus 1L_u$, $\ominus 2C_{\parallel}$, $\oplus 1.5C_{\parallel}$, $\boxtimes 2L_u$, $\boxminus 2L_f$, $\oplus 2P$.

between the block–substrate interactions, and its ratio with χ_{AB} is a good way to illustrate the relative strength of the substrate selectivity. In Figs. 5 and 6, $|\Delta/\chi_{AB}|$ ranged between 0.2 and 0.4 corresponds to a fairly weak interaction between the blocks and substrates. Reversed surface preference ($\Delta N = \pm 8.0$) leads to two completely different phase diagrams, because the block copolymer itself is not symmetric. The vertical axis of these diagrams denotes $\chi_{AB}N$, while the horizontal axis denotes the thickness of the film in the unit of R_{Gauss} . When the film thickness $\Delta < 1.2R_{Gauss}$, the C_{\perp} phases are dominant on the left boundary of both phase diagrams. The surface preference of the substrates is not strong enough to attract enough A to cover the surfaces, while the entropic energy increases to adapt the film thickness if a C_{\parallel} phase occurred. With the increase of the film thickness, both the diagrams show an obvious alternation between two types of morphologies. In Fig. 5 the alternation is between the C_{\parallel} and C_{\perp} phases; while in Fig. 6 it is between the C_{\parallel} and L phases.

The difference between Figs. 5 and 6 is, however, much more evident. A large region of the L (including L_f and L_u) and

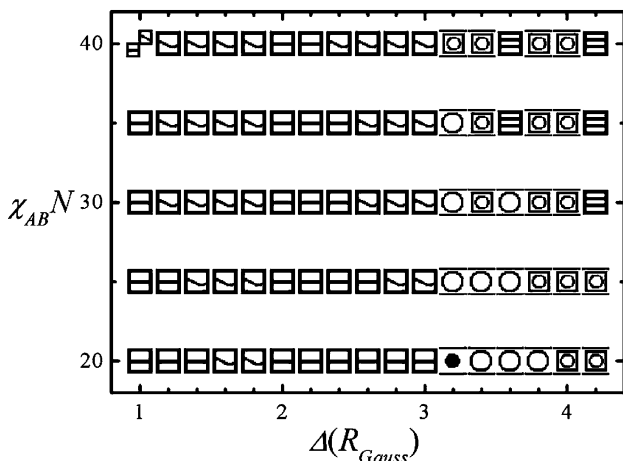


Fig. 8. Phase diagram for $\Delta N = 40.0$. $\boxplus 1L_f$, $\boxplus 1L_u$, $\boxminus 2L_f$, $\boxtimes LC$, $\ominus LS$, $\bullet LP$, $\boxtimes 1L_f$ and $1L_u$ with the same free energy.

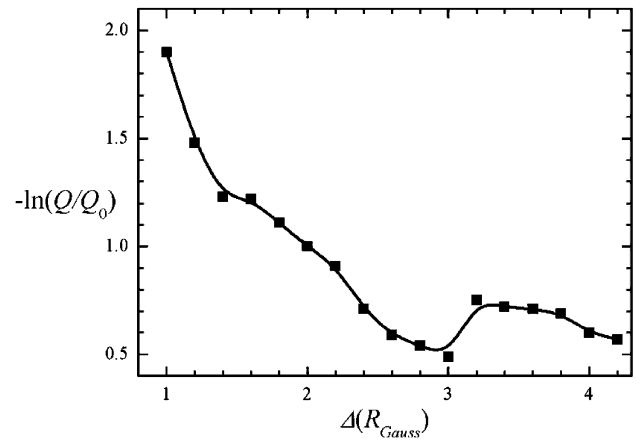


Fig. 9. The entropic free energy when $\chi N = 25$, $\Delta N = 8.0$, $f = 0.3$.

P phases in Fig. 6, which are thermodynamically stable, completely disappears in Fig. 5. On the other hand, in Fig. 5, a wide region of C_{\perp} phase exists as the film thickness approximated to $3R_{Gauss}$, but it is not found in Fig. 6.

Two important factors can affect the phase diagram of the confined cylindrical block copolymers. One is the preference of the two surfaces of the substrates. When the surface attraction is not strong enough to overpower the entropic energy to create a wetting layer of one species, the system will compromise on cylinders (C_{\perp} or C_{\parallel}) with slight deformation near the surfaces. A similar deformation was seen in linear triblock copolymer thin films [47]. For the C_{\perp} phases under different surface selectivity in Fig. 1, when $\Delta < 0$, the A–B interfaces shrink near the substrate surfaces, which makes the cylinders look like ellipses; while for $\Delta > 0$, the A–B interfaces expands. Similar deformation occurs for the C_{\parallel} phases, too. In other words, near the interfaces lamellae are always preferred in terms of surface interaction energy. To qualitatively analyze the surface energy for C_{\perp} , C_{\parallel} , and L phases, we ignore the slight distortion of the cylinders near the substrates, which means the fraction of the species A is 0.3 for the C_{\perp} phase and 0.50 or 0.58 for the C_{\parallel} phases (assuming that the parallel cylinders are packed in a hexagonal lattice) near the A-selective substrates (with $\Delta > 0$), and the fraction of the species B is 0.7 for the C_{\perp} phase and approaching to 1 for the C_{\parallel} phases (we only consider $1C_{\parallel}$ and $2C_{\parallel}$ in Fig. 1) near the B-selective substrates (with $\Delta < 0$). The fraction of the selected species in lamellae phases is always equal to 1. Suppose the surface interaction energy between the substrate and attracted species is $-\sigma$ ($\sigma > 0$) per unit area, and the that between the substrate and repulsed segment is σ , then the fraction of the surface energy of the different structures for the A-selective substrates is,

$$\begin{aligned} F_{\text{surface}}(C_{\perp}) : F_{\text{surface}}(C_{\parallel}) : F_{\text{surface}}(L) \\ &= (0.3(-\sigma) + 0.7\sigma) \\ &: (0.5(-\sigma) + 0.5\sigma) : (1(-\sigma) + 0\sigma) \\ &= 0.4 : 0 : -1 \end{aligned}$$

The fraction of the surface energy for the B-selective substrates is,

$$\begin{aligned} F_{\text{surface}}(C_{\perp}) : F_{\text{surface}}(C_{\parallel}) : F_{\text{surface}}(L) \\ = (0.7(-\sigma) + 0.3\sigma) : (1(-\sigma) + 0\sigma) \\ : (1(-\sigma) + 0\sigma) = -0.4 : -1 : -1 \end{aligned}$$

This estimation reveals why lamellae disappear in Fig. 5 but dominate in Fig. 6. When $\Delta > 0$, the substrates attract the minority and repel the majority, the surface energy goes against C_{\perp} and has not much incline to C_{\parallel} . But it strongly prefers lamellar phase for the complete cover of the minority species A. So the phase diagram shows the competition between the C_{\parallel} and L phases (Fig. 6, $\Delta > 0$). When $\Delta < 0$, the substrates attract majority B species, lamellae no longer have advantage over C_{\parallel} on surface energy. Then the phase diagram shows the alternation of the C_{\parallel} and C_{\perp} phases (Fig. 5, $\Delta < 0$) (Fig. 10).

The second factor comes from the confinement. Using density functional calculations, Huinink et al. have found that for the neutral substrates there is a slight preference for the shorter block [38]. Confined between two neutral surfaces, the film alternates between C_{\parallel} and C_{\perp} . But under a slight

preference of the longer block, C_{\perp} always happens. Wang et al. observed the same phenomenon in Monte-Carlo simulations [39]. They attributed this effect to the enrichment of the chain ends near a hard and flat surface. The fraction of the chain ends of type A is 0.5, larger than the fraction of the segment A in the whole system. Therefore, the chain ends enriched near the surface result in an apparently slight preference of the neutral surfaces for the A block. It is a purely entropic effect. To validate this confinement effect, we search a typical case of $\chi_{AB}N=20$. When the substrates are neutral, only the perpendicular cylindrical phase is stable with a period that is same as that of the bulk phase. In Fig. 11, we plot the free energy difference (per polymer chain) of the possible C_{\parallel} phases and the C_{\perp} phase when $\Delta N=0.0$ and -4.4 . The beeline with zero value denotes the C_{\perp} phase. The free energies for the $1C_{\parallel}$ and $2C_{\parallel}$ phases vary with the film thickness. In Fig. 10(a), when $\Delta N=0.0$, the intersection of these free energy curves indicates the alternating existence of these structures as the film thickness increases, which means, for cylindrical phases, neutral substrates are actually not neutral (because the perpendicular phase is not always stable). In the confined symmetric diblock copolymers system, perpendicular lamellae are always stable for neutral substrates). In Fig. 10(b), when $\Delta N=-4.4$ (which means the substrates attract the longer blocks B, and $|\Delta/\chi_{AB}|=0.22$. This result agrees with that of Wang et al., in Ref. [39].), the free energy for C_{\perp} is always the minimum. The substrate surface preference for the longer blocks has countervailed the confinement induced entropic preference for the shorter blocks. Thus C_{\perp} is the only structure occurred under this condition. This entropic effect hastens the existence of the lamellae structure in Fig. 6, too, and the region of lamellae phase broadens as $\chi_{AB}N$ increases. If ΔN is slightly smaller than -4.4 , the alternation between C_{\perp} and C_{\parallel} (b) exists.

Now we turn to discuss the new phases: undulated cylinders, undulated lamellae and parallel cylinders with non-integer period ($1.5C_{\parallel}$). These phases have never been reported in previous simulations in confined films. The undulated cylinders and $1.5C_{\parallel}$ only occur in Fig. 5 where the substrates have a weak favor for B blocks.

In Fig. 5 (in which the substrates favor the B blocks), with the film thickness varying from $1.6R_{\text{Gauss}}$ to $2R_{\text{Gauss}}$, there is a region of the undulated cylindrical (C_u) structure. The peaks of the neighboring cylinders are interlaced. It is a transitional structure between C_{\perp} and $1C_{\parallel}$. The cylinders (of the A blocks) contort to adapt to the film thickness while doing the best to reduce the possible contacts of the A segments and the substrates to decrease the unfavorable surface energy. The undulated cylinder structure is thermodynamically stable in the parameter region shown in Fig. 5.

In Fig. 6, we find contorted lamellae near the boundary of the flat lamellae regions. The waves in the undulated lamellae (L_u) are usually arranged in two types, either in striation or in square, as shown in Fig. 2. In the present stage, we are not able to determine which pattern is more stable, because the existence of these structures depends on the simulation box size and their free energies are too close, beyond the precision

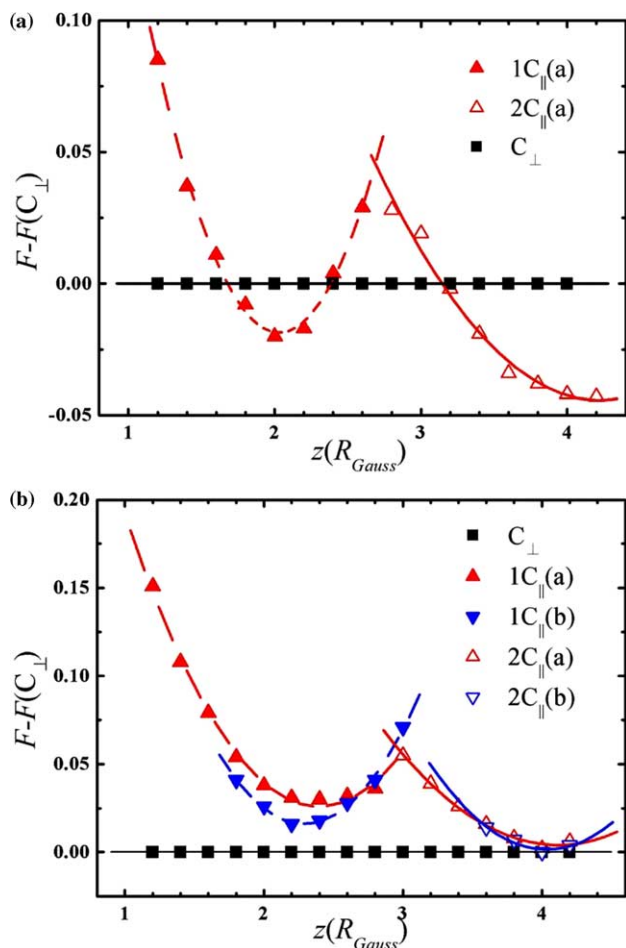


Fig. 10. Free energy difference of perpendicular and parallel cylinders for the diblock copolymer with $f=0.3$, $N=50$ and $\chi_{AB}=20$. F is the free energy per chain with $k_B T=1$ and statistical segment length $a=1/\sqrt{2}$. (a) $\Delta N=0.0$; (b) $\Delta N=-4.4$.

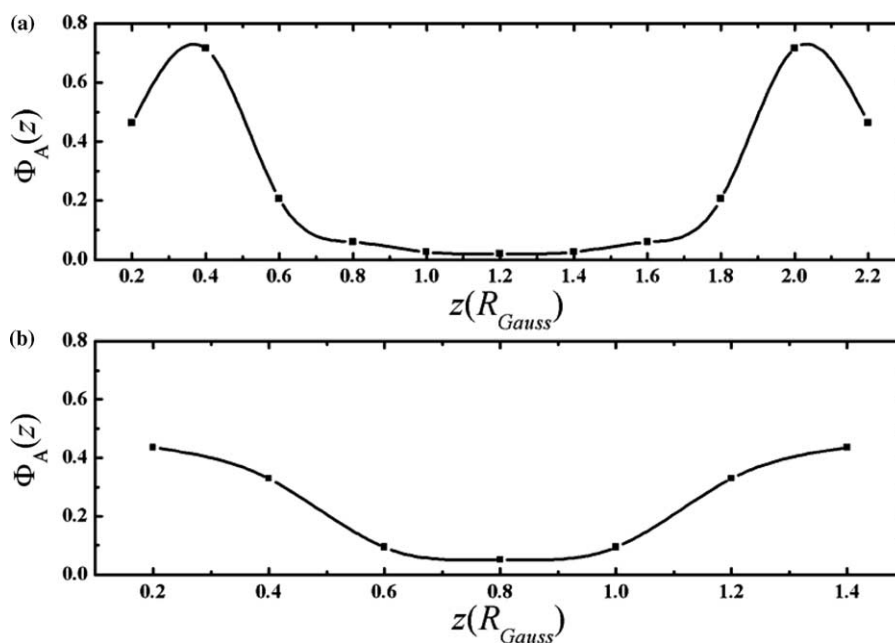


Fig. 11. Density profiles of the species A along the z -axis with, for the film thickness (a) $\chi_{AB}N=20$, $\Delta N=40.0$ for the film thickness (a) $\Delta=2.2R_{\text{Gauss}}$ and (b) $\Delta=1.4R_{\text{Gauss}}$.

of the calculation (within 10^{-6}). However, what we are sure is that in this region only the waved lamellae structures are thermodynamically stable because both of their free energies are lower than any other structures. The lamellae become concavo–convex to cope with the film thickness, which resembles the distortion of lamellae under external strain [52].

According to the previous work on distorted lamellae [52], the periods of the undulations depend non-linearly on χ_{AB} , N , f and film thickness Δ . It is more complex under the confinement and absorption condition. Hence we will not discuss the periods of undulated morphologies here.

Another new structure is the $1.5C_{\parallel}$ phase. The symmetric substrates are able to induce asymmetric surface patterns (one surface is covered by a stripe pattern of alternating A and B components while another is covered only by the B segments). Actually, $1.5C_{\parallel}$ is an intermediate state in between $1C_{\parallel}$ and $2C_{\parallel}$ and only exists in a narrow region in the phase diagram.

At last we note that in Figs. 5 and 6 there are regions where the hybrid structures are stable. Typical types of these hybrid structures are shown in Fig. 4. Usually, at a particular point in the H-region, there can be several types of hybrid structures, each has the free energy lower than any other pure structures. There are too many possible combination of these structures [47], and the free energy differences among these mixed phases sometimes are too small to identifying which one is the most stable. Therefore, we did not draw the detailed structure of the H-region in Fig. 6, in which the simulation results include LP, PC, LPC, etc.

3.2. Strong substrate preference

In Figs. 7 and 8, the ratio $|\Delta/\chi_{AB}|$ ranges between 1.0 and 2.0 when $\Delta N = \pm 40.0$. Under this condition, the substrates are always covered with their preferred species, we,

therefore, define it to be the strong substrate preference condition. In other words, at any point on the surface layer, the volume fraction of the attracted species is always much higher than the repelled one. Since the thin films in experiments usually have a cover of one component on surfaces, we consider them to be quenched under strong substrate preference, thus a corresponding position in our diagrams can be found for the nanostructures observed in experiments. For example, in Ref. [34], the poly(styrene-*b*-butadiene) diblock copolymers has $f=0.266$ and the cylinder–cylinder distance D_0 in bulk is 21.9 nm. Thin films of this kind of block copolymers show one layer perforated lamellae (1P) structure at 25–27 nm film thickness ($\sim 1D_0$) and two layer perforated lamella (2P) at about 45 nm film thickness ($\sim 2D_0$). The substrates are in favor of segment B. In our simulation the bulk cylinder–cylinder distance $D_0 \approx 2.3R_{\text{Gauss}}$ when $\chi_{AB}=20$. Correspondingly, in Fig. 7, there are 1P at film thickness $\Delta=2R_{\text{Gauss}}$ or $2.4R_{\text{Gauss}}$ ($\sim 1D_0$) and 2P at $\Delta=4.2R_{\text{Gauss}}$ ($\sim 2D_0$) for $\chi_{AB}N=20$. Radzilowski et al. found an interesting lamellae structure while observing the cross-section of the thin film with $f=0.325$ and strong short block preference on the substrates. They saw ‘hemispherical PB domains (PB is the minority component) attached to either PB surface layer’, where the film thickness is about 25 nm ($\Delta/D_0 \approx 0.72$). We believe that what they observed might be the undulated lamellae because we found L_u when $\chi_{AB}N=20$ and $\Delta=1.6$ – $1.8R_{\text{Gauss}}$ ($\Delta/D_0 \approx 0.77$).

With the effect of strong block–substrate energy and entropic preference of the segment A, in a broad region of the phase diagram in Fig. 8, lamellae are stable. The rest is mixed phases in which one of the structures is lamellae phase. As the film thickness increases, the hybrid structures are arranged in LS, LC, and LP. If we remove the surface layers of

the lamellae phase (wetting layer), it arranges as S, C, and P, just like the series in bulk system with the increase of volume fraction of the A block. This provides us a hint that it might be the relative amount of the A blocks in the center region of the film that decides the morphology under strong substrate preference for the shorter block A.

In the phase diagram of Fig. 8 where the substrates attract the minority A species, there are two $1L_f$ regions with a L_u phase sandwiched in between. These two $1L_f$ structures have different concentration of the A blocks along the thickness. Fig. 11 shows the density profile of the A species along the z -direction with $\chi_{AB}N=20$ and film thickness $\Delta=1.4R_{\text{Gauss}}$ and $2.2R_{\text{Gauss}}$, respectively. For $\Delta=2.2R_{\text{Gauss}}$, the A blocks segregate intensively at the substrate surfaces and the interface between the A and B domains is sharp (the density Φ_A drops at $z=0.2R_{\text{Gauss}}$ and $2.2R_{\text{Gauss}}$, because we have the incompressibility at surface as $\Phi_A + \Phi_B = 1/2$, defined in Eq. (5)). For $\Delta=1.4R_{\text{Gauss}}$, however, Φ_A has never exceeded 0.5 and the A–B interface is wider, showing a weak segregation. This lamellar structure stems from the improper film thickness and the overpowering surface attraction of the A blocks. This weak-segregated phase was called a disorder phase with wetting layers in previous works [44–47,49].

The phase diagram for $\Delta N = -40$ (substrates attract the B blocks, Fig. 7) is similar to that for $\Delta N = 8.0$ in terms of the alternation between the C_{\parallel} and L phases. Under such strong surface selectivity, the system prefers C_{\parallel} other than C_{\perp} . At the left part of the phase diagram, a large region of $1C_{\parallel}$ phase emerges, although the film thickness there cannot accommodate even one cylinder. Fig. 1(c) ($1C_{\parallel}$) shows the morphology under this condition. The hard walls compress the cylinders into a narrow space where the film thickness is less than $1.6R_{\text{Gauss}}$.

3.3. Cylinder–lamella transition

A cylindrical phase of block copolymers (in bulk) can transform into lamellae structure when confined between selective surfaces. This transition between cylindrical and lamellar phases in thin films are predicted by different theories [8,38,39] and has been observed in experiments [24–27].

At first let us take the system with $\chi_{AB}N=30$, $N=50$, and $f_A=0.3$ as an example to identify the optimal period that reaches the lowest free energy for the lamellae phase. This is achieved by importing the density profile of the lamellae structure as the initial fields. The free energy of the lamellae with different period L is obtained by changing the calculation box. We compare the free energy in Fig. 12 and find the position of the minimum of the fitted quadratic curve is located at $L \approx 2.3R_{\text{Gauss}}$. Indeed, at the corresponding positions in Figs. 6–8, where $\chi_{AB}N=30$, $\Delta=2.2R_{\text{Gauss}}$ and $2.4R_{\text{Gauss}}$, there exists the L_f structure. And near the doubled film thickness ($\Delta=4.2R_{\text{Gauss}}$) flat lamellae phase ($2L_f$) again are stable. Thus we draw the conclusion: confined thin films with sufficient substrate selectivity will lead an otherwise cylindrical phase to a lamellar structure when the film thickness fits the optimal period of the lamellae. Note that the $1L_f$ region on the left of

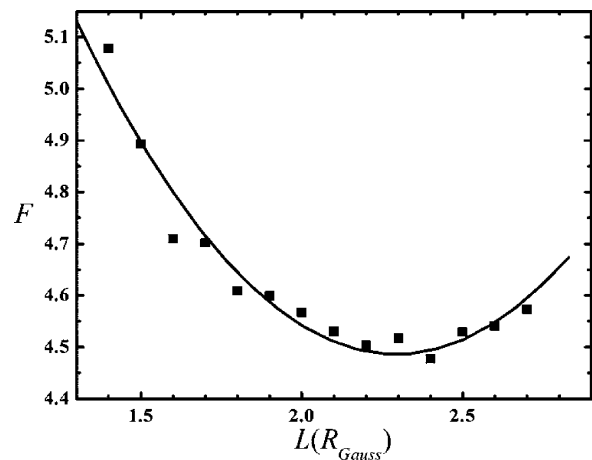


Fig. 12. Free energy of the lamellar phase with different period (fitted by a quadratic curve) as $f=0.3$, $N=50$ and $\chi_{AB}N=30$. L is the period of lamellar structure in unit of R_{Gauss} . F is the free energy per chain calculated by SCFT simulation taking $k_B T=1$ and $a=1/\sqrt{2}$.

Fig. 8 is different from the others in its origin, as we have explained in the previous section.

The morphology seldom transits directly from cylinders to flat lamellae. Actually, such transition always occurs gradually. Huinink et al. had noticed this phenomenon and concluded that there are two separate transition between C_{\parallel} and L_f : it has to be C_{\parallel} –P transition and P– L_f transition [40]. According to our results, however, there can be three more transitions: P– L_u transition, L_u – L_f transition and L_u – C_{\parallel} transition.

Take the system with $\chi N=35$ as an example (Fig. 6), increasing the film thickness starting from $\Delta=1.4R_{\text{Gauss}}$, a series of transformation happens as $1C_{\parallel}$ – $1P$ – $1L_f$ – $1L_u$ – H – $2L_u$ – $2L_f$. The $1L_f$ region is sandwiched between $1P$ and $1L_u$. Thus the L_u – L_f transition occurs. In Fig. 7, from $\Delta=1.8R_{\text{Gauss}}$, the series is $1P$ – $1L_u$ – $1L_f$ – $1L_u$ – $1C_{\parallel}$ – $2L_u$ – $2P$ – $2L_f$. Two $1L_u$ phases occur on each side of $1L_f$. Here we have all of L_u – L_f , L_u –P and L_u – C_{\parallel} transitions. In Fig. 8, from $\Delta=1.2R_{\text{Gauss}}$ to $\Delta=3R_{\text{Gauss}}$, it is $1L_u$ – $1L_f$ – $1L_u$. There is L_u – L_f transition again.

In the diagrams, L_u phase has a wide enough area and the phase transitions between L_u and L_f , P or C_{\parallel} often occur. But the L_u structure requests a strict confinement condition. However, the transition between L_u and other structures may not easy to be observed in the most experiments because the films prepared often have at least one surface unconfined, which relaxed the confinement effect.

4. Conclusions

We have used real-space SCFT simulation to reveal possible morphology of an asymmetric AB diblock copolymer confined between two homogeneous hard walls. The volume fraction of the A block is fixed to be $f=0.3$. Although many previous simulations have been performed [8,37–49], this relatively simple system still shows a much intriguing behavior. We have found that, under confinement, in addition to the reported structures (parallel and perpendicular cylinders, flat lamellae, perforated lamellae), undulated cylinders and undulated

lamellae and parallel cylinders with non-integer period are also stable due to the block–substrate interactions. By systematically varying the film thickness and the interaction parameters between the two blocks, phase diagrams are constructed for typical block–substrate interactions. We compare the phase diagrams for weak and strong substrate preferences and discuss the effects of confinement and substrate preference on the stability of various structures. Our main conclusions are as follows.

- (1) A variety of structures are found to be stable under confinement, such as flat lamellae (L_f), perpendicular cylinders (C_{\perp}), parallel cylinders with integer layers (C_{\parallel}), perforated lamellae (P), and hybrid structures (H). They are widely observed both in experiment and theory works. Moreover, we find three new structures in our simulation, i.e. undulated lamellae (L_u), undulated cylinders (C_u), and parallel cylinders with non-integer period ($1.5C_{\parallel}$), are observed with particular film thickness and block–substrate interaction. These new morphology inquires strict confinement on each side of the film and two cylinder structures (C_u and $1.5C_{\parallel}$) ask for an ultra thin film thickness between $1.6R_{\text{Gauss}}$ and $2.8R_{\text{Gauss}}$ and weak substrate preference for the longer blocks (Fig. 5). The $1.5C_{\parallel}$ phase comes out only when the repulsive interaction between the two blocks is strong enough ($\chi N > 30$). It is rather interesting if we aware that the two surfaces are symmetric.
- (2) Under weak preferences, the phase diagram shows an alternation between the C_{\parallel} and C_{\perp} phases when the substrates absorb the longer block (Fig. 5); while it shows an alternation between the C_{\parallel} and L phases when substrates absorb the shorter block (Fig. 6). Under strong preferences, the absorbed segments covered the whole substrates (Figs. 7 and 8). L phases are dominant when shorter block is preferred near substrates (Fig. 8); while an arrangement of L, P and C phases in the diagram when longer block is preferred near the substrates (Fig. 7). The L_f phase is expected when the film thickness fits the optimal period of lamellae (except when the substrates have a weak preference for the longer block).
- (3) Confined thin films with sufficient substrate selectivity will lead an otherwise cylindrical phase to a lamellar phase when the film thickness fits the optimal period of the lamellae. However, increasing the film thickness seldom causes the morphology transit directly from cylinders to flat lamellae—there are always transitional phases in between.

Acknowledgements

We gratefully acknowledge the financial support from the National Basic Research Program of China (2005CB623807), and the NSF of China (Grant Nos. 20221402, 20234010, 20374016, and 20490220). F.Q. acknowledges the Ministry

of Education of China (FANEDD 200225) and STCSM (Grant No. 02QE14010).

References

- [1] Lambooy P, Russell TP. *Phys Rev Lett* 1994;72:2899–902.
- [2] Russell TP, Lambooy P, Kellogg GJ, Mayes AM. *Physica B* 1995; 213/214:22–5.
- [3] Koneripalli N, Singh N, Levicky R, Bates FS, Gallagher PD, Satija SK. *Macromolecules* 1995;28:2897–904.
- [4] Koneripalli N, Levicky R, Bates FS, Ankner J, Kaiser H, Satija SK. *Langmuir* 1996;12:6681–90.
- [5] Kellogg GJ, Walton DG, Mayes AM, Lambooy P, Russell TP, Gallagher PD, et al. *Phys Rev Lett* 1996;76:2503–6.
- [6] Huang E, Russell TP, Harrison C, Chaikin PM, Register RA, Hawker CJ, et al. *Macromolecules* 1998;31:7641–50.
- [7] Lee S-H, Kang H, Kim YS, Char K. *Macromolecules* 2003;36:4907–15.
- [8] Brown G, Chakrabarti A. *J Chem Phys* 1994;101:3310–7.
- [9] Kikuchi M, Binder K. *J Chem Phys* 1994;101:3367–77.
- [10] Geisinger T, Müller M, Binder K. *J Chem Phys* 1999;111:5241–50.
- [11] Geisinger T, Müller M, Binder K. *J Chem Phys* 1999;111:5251–8.
- [12] Sommer J-U, Hoffmann A, Blumen A. *J Chem Phys* 1999;111:3728–32.
- [13] Wang Q, Yan Q, Nealey PF, de Pablo JJ. *J Chem Phys* 2000;112:450–64.
- [14] Frischknecht AL, Curro JG, Frink LJD. *J Chem Phys* 2002;117: 10398–411.
- [15] Shull KR. *Macromolecules* 1992;25:2122–33.
- [16] Turner MS. *Phys Rev Lett* 1992;69:1788–91.
- [17] Wong KY, Trache M, McMullen WE. *J Chem Phys* 1994;101:5372–87.
- [18] Walton DG, Kellogg GJ, Mayes AM, Lambooy P, Russell TP. *Macromolecules* 1994;27:6225–8.
- [19] Milner ST, Morse DC. *Phys Rev E* 1996;54:3793–810.
- [20] Matsen MW. *J Chem Phys* 1997;106:7781–91.
- [21] Pickett GT, Balazs AC. *Macromolecules* 1997;30:3097–103.
- [22] Tang WH. *Macromolecules* 2000;33:1370–84.
- [23] Fasolka MJ, Banerjee P, Mayes AM, Pickett G, Balazs AC. *Macromolecules* 2000;33:5702–12.
- [24] Karim A, Singh N, Sikka M, Bates FS, Dozier WD, Felcher GP. *J Chem Phys* 1994;100:1620–9.
- [25] Liu Y, Zhao W, Zheng X, King A, Singh A, Rafailovich MH, et al. *Macromolecules* 1994;27:4000–10.
- [26] Harrison C, Park M, Chaikin P, Register RA, Adamson DH, Yao N. *Macromolecules* 1998;31:2185–9.
- [27] Harrison C, Park M, Chaikin P, Register RA, Adamson DH, Yao N. *Polymer* 1998;38:2733–44.
- [28] Thum-Albrecht T, Steiner R, DeRouchey J, Stafford CM, Huang E, Bal M, et al. *Adv Mater* 2000;12:787–91.
- [29] Lammertink RGH, Hempenius MA, Vancso GJ. *Langmuir* 2000;16: 6245–52.
- [30] Yokoyama H, Mates TE, Kramer EJ. *Macromolecules* 2000;33: 1888–98.
- [31] Fasolka MJ, Banerjee P, Mayes AM, Pickett G, Balazs AC. *Macromolecules* 2000;33:5702–12.
- [32] Lammertink RGH, Hempenius MA, Vancso GJ, Shin K, Rafailovich MH, Sokolov J. *Macromolecules* 2001;34:942–50.
- [33] Segalman RA, Hexemer A, Kramer EJ. *Macromolecules* 2003;36: 6831–9.
- [34] Radzilowski LH, Carvalho BL, Thomas EL. *J Polym Sci, Part B* 1996;34: 3081–93.
- [35] Konrad M, Knoll A, Krausch G, Magerle R. *Macromolecules* 2000;33: 5518–23.
- [36] Zhao J, Jiang S, Ji X, An L, Jiang B. *Polymer* 2005;46:6513–21.
- [37] Suh KY, Kim YS, Lee HH. *J Chem Phys* 1998;108:1253–6.
- [38] Huinink HP, Brokken-Zijp JCM, van Dijk MA, Sevink GJA. *J Chem Phys* 2000;112:2452–62.
- [39] Wang Q, Nealey PF, de Pablo JJ. *Macromolecules* 2001;34:3458–70.
- [40] Huinink HP, van Dijk MA, Brokken-Zijp JCM, Sevink GJA. *Macromolecules* 2001;34:5325–30.

- [41] Pereira GG. *Phys Rev E* 2001;63:061809.
- [42] Wang Q, Nealey PF, de Pablo JJ. *Macromolecules* 2003;36:1731–40.
- [43] Podariu I, Chakrabarti A. *J Chem Phys* 2003;118:11249–57.
- [44] Knoll A, Horvat A, Lyakhova KS, Krausch G, Sevink GJA, Zvelindovsky AV, et al. *Phys Rev Lett* 2002;89:035501.
- [45] Sevink GJA, Fraaije JGEM, Huinink HP. *Macromolecules* 2002;35:1848–59.
- [46] Horvat A, Lyakhova KS, Sevink GJA, Zvelindovsky AV, Magerle R. *J Chem Phys* 2004;120:1117–26.
- [47] Lyakhova KS, Sevink GJA, Zvelindovsky AV, Horvat A, Magerle R. *J Chem Phys* 2004;120:1127–37.
- [48] Knoll A, Lyakhova KS, Horvat A, Krausch G, Sevink GJA, Zvelindovsky AV, et al. *Nat Mater* 2004;3:886–90.
- [49] Ludwigs S, Krausch G, Magerle R, Zvelindovsky AV, Sevink GJA. *Macromolecules* 2005;38:1859–67.
- [50] Drolet F, Fredrickson GH. *Phys Rev Lett* 1999;83:4317–20.
- [51] Matsen MW, Bates FS. *Macromolecules* 1996;29:1091–8.
- [52] Wang ZG. *J Chem Phys* 1994;100:2298–309.